Patterning Lead Zirconate Titanate Nanostructures at Sub-200-nm Resolution by Soft Confocal Imprint Lithography and Nanotransfer Molding

Sajid U. Khan, Ole F. Göbel, Dave H. A. Blank, and Johan E. ten Elshof*

MESA+ Institute for Nanotechnology, University of Twente, P.O. Box 217, 7500 AE Enschede, The Netherlands

ABSTRACT Patterned sol−gel-derived lead zirconate titanate (PZT) thin films with lateral resolutions down to 100 nm on silicon are reported. Both an imprint and a transfer-molding method were employed. The formed patterns after annealing were characterized with scanning electron microscopy, atomic force microscopy, and X-ray diffraction. Despite the small dimensions and flexibility of the poly(dimethylsiloxane) (PDMS) stamps used for patterning, the quality of replication was found to be good. The influence of the surface energies of the substrate, PDMS mold, and precursor solution on the quality of pattern replication is discussed. The colloidal structure of the PZT sol−gels from which the patterns were made was studied with small-angle X-ray scattering. The sols were found to be chemically homogeneous down to a length scale of ∼2 nm and higher, which is sufficient for pattern replication on ∼100 nm scale.

KEYWORDS: soft lithography • sol−gel • patterning • PZT • lead zirconate titanate • SAXS

INTRODUCTION

The fabrication of nanometer-scale structures of functional oxides is an important issue in modern materials science and technology. Among these oxides, ferroelectric oxide thin films and functional patterns are of great importance because of their physically and technologically important properties, such as spontaneous polarization, high dielectric constant, and piezo- and pyroelectricity (1−3). The ability to pattern functional oxides with nanometer-scale resolution is desirable for application in modern miniaturized systems, e.g., sensors, actuators, or information storage media (1). While conventional photolithographic techniques are expensive and have certain limitations for patterning oxide materials (4, 5), the so-called soft-lithographic techniques, developed in the Whitesides group at Harvard University, may be used alternatively because of their versatility, technical simplicity, and low cost (4). These techniques can be combined with the use of sol−gel-based precursors to yield materials such as lead zirconate titanate (PZT).

Soft lithography has been utilized by several research groups to micropattern a variety of oxide materials (6−9). PZT has been patterned from sol−gel precursor solutions by Micromolding in Capillaries (MIMIC) (10, 11), a soft-lithographic technique with which patterns can be formed on micrometer and submicrometer length scales. Martin and Aksay observed nonuniform shrinkage across patterned PZT films with 2−20 μm resolution, resulting in "double-peak" film topographies whereby the film thickness was greater at the lateral edges than in the middle (11). The effect was explained in terms of accelerated drying rates in the corners of the replicated pattern. As the lateral feature sizes of the structures to be patterned diminish, this effect is expected to become less pronounced. However, MIMIC is not efficient for submicrometer-sized channels because friction from the channel walls prevents penetration of the precursor solution by capillary force in narrow channels. MIMIC is also easily disturbed by local contaminants with low surface energy. Fabrication techniques such as soft-lithographic micromolding and nanoimprint lithography are therefore more often considered for smaller feature sizes. It has been shown possible to pattern 350 nm PZT features by nanoimprint lithography using poly(dimethylsiloxane) (PDMS) as a stamp (12). Hampton et al. communicated the imprinting of various oxides at ∼500 nm lateral resolution with a perfluoropolyether elastomer master (13). Hitherto, soft-lithographic patterning of PZT with resolutions below 200 nm has not been reported. We employed soft confocal imprint lithography (SCIL) (14) with flexible PDMS molds. The process is schematically shown in Figure 1a. Because an imprint is made in a preformed deformable film, some residue layer will usually stay between patterned features. An alternative to imprint lithography is transfer lithography, schematically depicted in Figure 1b. We termed this process nanotransfer molding (NTM). It is equivalent to microtransfer molding but operates on the nanometer scale. The use of microtransfer molding has only been reported a few times for the patterning of functional oxides on the micrometer scale (15−17). The SCIL and NTM processes will be compared. It will be
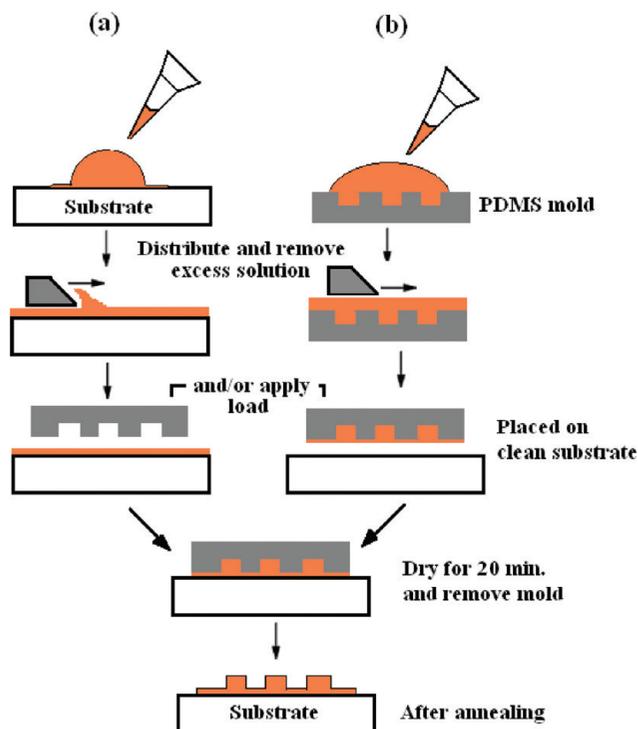
FIGURE 1. Schematic illustration of the modified patterning techniques: (a) SCIL; (b) NTM.

demonstrated that PDMS can be used to imprint and transfer PZT patterns with 100 nm lateral features without shape distortion of the flexible stamp, even when some external pressure is applied.

EXPERIMENTAL SECTION

PZT Synthesis. Lead(II) acetate trihydrate (99%, Aldrich), zirconium(IV) *n*-propoxide (70% w/w in *n*-propanol, Alfa Aesar), and titanium(IV) isopropoxide (99.99%, Aldrich) were used as precursors. Glacial acetic acid (99.8%, Merck) and 2-methoxyethanol (>99.3%, Aldrich) were used as solvents. The PZT solution was prepared following sol−gel recipes described in detail elsewhere (18, 19). Essentially, two separate stock solutions were made. One of them is a solution of lead acetate in glacial acetic acid; the other one is a mixture of zirconium and titanium isopropoxides in 2-methoxyethanol in a 52:48 molar ratio. After removal of all residual water from the lead acetate solution by refluxing at 105 °C, the stock solutions were mixed in an appropriate molar ratio. The concentration of PZT in the final solution was kept at 0.6 M. A molar excess of lead acetate of 15 mol % was added in order to compensate for the Pb loss during thermal annealing.

Nanopatterning Experiments. Two techniques were employed in the present work to pattern PZT from a sol−gel precursor solution. They are shown in Figure 1. In the SCIL process (14) shown in Figure 1a, a drop of the PZT sol was placed on a Si(100) substrate and homogenously distributed, e.g., by casting or spin-casting with 500−1000 rpm. Then a patterned PDMS mold was gently placed on the wet film and dried on a hot plate at 80 °C for 15−30 min. All PDMS molds were made from Sylgard 184 (Dow Corning Inc.) and cured at 60 °C for 24 h. The lateral resolution of the features in the PDMS stamps was 150−400 nm. The feature depth was 100 nm in all cases. The advantages of using a soft PDMS mold are that it provides good conformal contact, has a low reactivity with organic materials, and can be removed easily from the replicated pattern without distortion of the pattern (20).

The second technique, shown in Figure 1b, is NTM. Here the PZT sol was poured onto a patterned PDMS mold, distributed homogenously, transferred to the substrate, and dried under conditions similar to those in SCIL. Excess material was in both cases removed either with a soft PDMS block or with a hard material, e.g., a steel block.

Small-Angle X-ray Scattering (SAXS) Analysis. SAXS was carried out using synchrotron radiation on the Dutch-Belgian DUBBLE beamline BM-26B of the ESRF in Grenoble, France (21), using a beam energy of 12 keV. The beam was focused on a corner of the 2D CCD detector to maximize the range of accessible q values. When the 2D detector of DUBBLE was placed at a distance of 1.5 m from the sample, the scattered intensity was measured for q (scattering vector) between 0.13 and 5.56 nm^{-1}. A beam stop was applied to shield the detector from the direct beam and to avoid saturation of the outgoing signal. The raw data were corrected for the pixel-dependent detector sensitivity and integrated for channels with the same q values. In a typical SAXS analysis, the scattering intensity I is plotted against the scattering vector Q (nm^{-1}), which is related to the scattering angle θ and the wavelength λ of the incident beam by $Q = 2\pi/\lambda \sin(2\theta)$. All measured solutions were contained in a capillary glass tube (Ø 1.5 mm, glass no. 14, Hildenberg, Malsfeld, Germany). The background signal, i.e., the scattering pattern of a capillary containing pure solvent or a mixture of solvents measured under the same conditions, was subtracted from the scattering pattern of the PZT sol.

X-ray Diffraction (XRD) and Atomic Force Microscopy (AFM) Analysis. XRD analysis was carried out with a Philips X'Pert diffractometer using Cu Kα radiation. AFM analysis was done with a Nanoscope IV (Veeco Instruments, Digital Instruments, Plainview, NY) in tapping mode.

RESULTS AND DISCUSSION

SAXS Analysis. Knowledge of the colloidal structure of the precursor solution is therefore of importance. The primary building blocks should be at least an order of magnitude smaller than the channels of the mold in order to be able to reproduce its features with a high fidelity. The chemical homogeneity and microstructure of the final sintered product are also affected by the shape and size of the PZT sols (19). PZT sols that are inhomogeneous on a length scale of ∼6 nm have been reported, which is a considerable value if 100 nm nanostructures are targeted (22). SAXS experiments were performed on both the lead- and titanium/zirconium-containing stock solutions and on the mixed PZT precursor solution. The log I−log Q Porod plots of the scattering curves of the stock solutions and a PZT precursor solution after background subtraction are shown in Figure 2. The scattering curve of the lead acetate stock solution showed no variation in intensity I with Q within experimental error. This indicates a homogeneous solution, as is indeed expected for lead acetate in acetic acid. On the other hand, zirconium/titanium alkoxide in a 2-methoxyethanol stock solution showed a clear variation in the scattering intensity, indicating the presence of nanometer-sized structures in the solution. The size and shape of these structures can be interpreted in terms of their radius of gyration R_g and fractal dimension D_f, respectively (23). The latter parameter relates the mass M and effective radius of gyration R_g of colloidal particles via $M \sim R_g^{D_f}$ (23−25). The scattering curve of the zirconium/titanium alkoxide solution could be fitted to the Teixeira function (24, 26, 27). From the best fit, the fractal
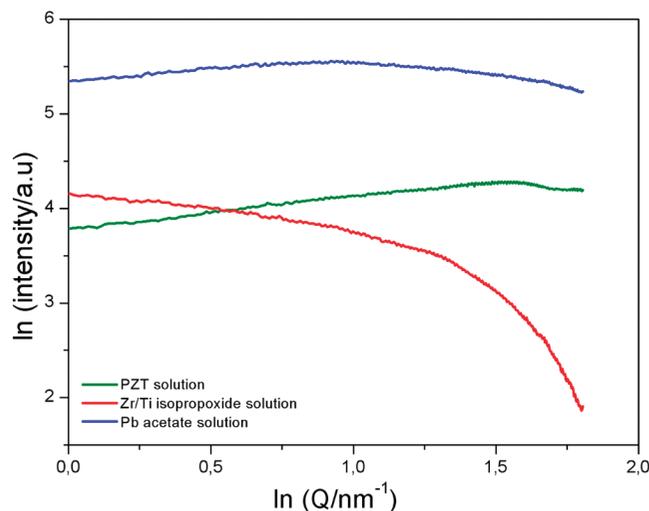
FIGURE 2. SAXS curves showing Porod plots of a solution of lead acetate in acetic acid (blue curve), a solution of zirconium and titanium isopropoxide in 2-methoxyetanol (red curve), and a stoichiometric PZT solution made by a mixing of the two separate solutions and aging (green curve).

correlation length ξ and fractal dimension D_f could be determined. The effective particle size in solution R_g can then be calculated from $R_g^2 = (1/2)D_f(D_f + 1)\xi^2$. The values of ξ and D_f in the zirconium/titanium stock solution were approximately 0.2 nm and 3, respectively. Thus, R_g is ca. 1.0 nm. The effective particle diameter in solution is ca. $2R_g \sim$ 2 nm. Reasonably similar values have been determined from SAXS on ethanol-based titania sols (24). The scattering curve of the PZT mixed solution did not show any structure either. This is caused by the fact that the scattering and absorption by the element lead overwhelms the scattering signal of any other entities present in solution, such as the zirconia/titania nanoparticles. If the lead ions would somehow have associated with these titania/zirconia sols, then a different scattering curve would have been observed for the PZT solution. Hence, the observed curve strongly suggests that the structure of the PZT precursor solution used in this work is composed of a mixture of heavily branched 2-nm-sized mixed zirconia/titania sol particles with a fractal dimension 3 and unassociated dissolved lead ions, probably coordinated by acetate and/or 2-methoxyethanol ligands. The precursor solution is therefore chemically homogeneous down to a length scale of $\sim$2 nm. This is much smaller than the features of the patterns to be formed and ensures chemical homogeneity in the final material.

Patterning Experiments. Marzolin et al. suggested that the liquid should spontaneously dewet the elastomer surface in imprinting processes such as SCIL, so that the protruding parts of the mold make conformal contact with the substrate and thus avoid a residual layer (28). This requires the surface tension of the precursor solution (γ_{sol}) to be larger than that of PDMS (γ_{PDMS}). The surface tensions of acetic acid and 2-methoxyethanol are 27.6 and 31.8 mJ/m^2 at 20 °C, respectively, so the surface tension of a PZT sol, γ_{sol}, will be around 30 mJ/m^2. The surface energy of PDMS, γ_{PDMS}, is 21.6 mJ/m^2. Hence, the sol is indeed expected to dewet the elastomer surface spontaneously.

In transfer-molding processes, the requirements on the surface energies of both the PDMS mold and the silicon substrate are more stringent. First of all, their surface energies should be such that PZT sols fill the features of the mold spontaneously, which implies that good wetting of the mold by the PZT sol is needed. So, γ_{sol} should be smaller than γ_{PDMS}. Furthermore, the sols should also adhere to the silicon substrate and then be released from the PDMS mold after initial drying (16). For proper demolding of the PZT precursor from the mold and adherence to the silicon substrate (with surface tension γ_{SiO_x}), the binding energy between PDMS and PZT should be smaller than the energy between the substrate and PZT. This means that $\gamma_{PDMS}A_{PDMS} < \gamma_{SiO_x}A_{SiO_x}$, where A_{SiO_x} and A_{PDMS} are the interfacial surface areas of the substrate and PDMS inside the mold, respectively. For rectangular channels with a height:width ratio of b, these surface areas are related via $A_{PDMS} = (2b + 1)A_{SiO_x}$. Hence, the full requirement for the patterning of line structures by NTM can be written as

$$\gamma_{sol} < \gamma_{PDMS} < 1/(2b + 1)\gamma_{SiO_x} \qquad (1)$$

The requirement implies that there is a theoretical upper limit to the aspect ratio b of the structure that can be patterned by NTM. Namely, $b < {}^{1}/_{2} (\gamma_{SiO_x}/\gamma_{sol} - 1)$. In the present work, the value of b varied between 0.25 and 0.7, which is well below the threshold. Because $\gamma_{sol} > \gamma_{PDMS}$, PDMS is not a priori suitable for NTM of PZT sols. However, when PDMS and silicon are treated in oxygen plasma, their surfaces become oxidized. This increases their surface energies, and thereby the polarity and hydrophilicity of these interfaces (29, 30). In the present work, plasma treatment (Harrick Plasma, 200 W) was carried out at a pressure of 80 Pa using molecular oxygen as the source. The surface energy of oxidized silicon is not known exactly but is expected to be higher than 103 mJ/m^2 (31). Hence, if the above-mentioned requirement eq 1 for transfer molding is satis-
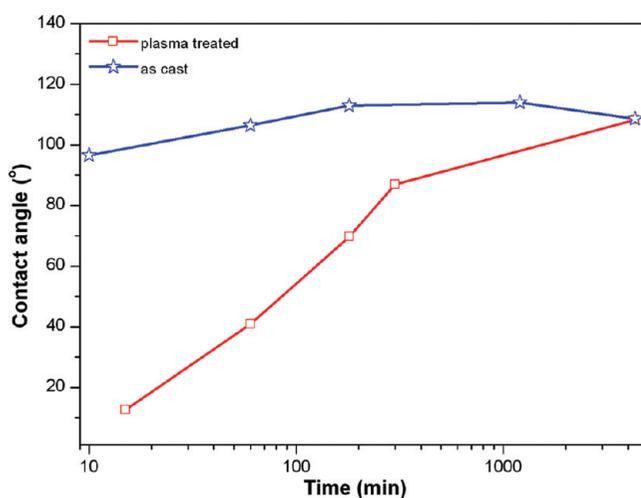

FIGURE 3. Change in the water contact angle on PDMS without (blue curve) and after (red curve) 2 min of oxygen plasma treatment. The PDMS samples were stored in a sealed Petri dish between measurements.
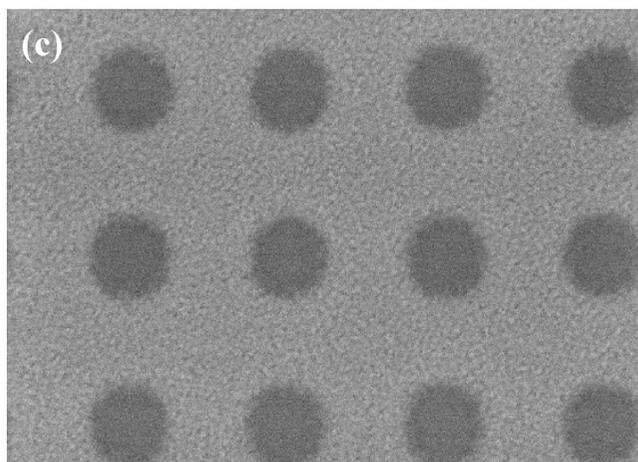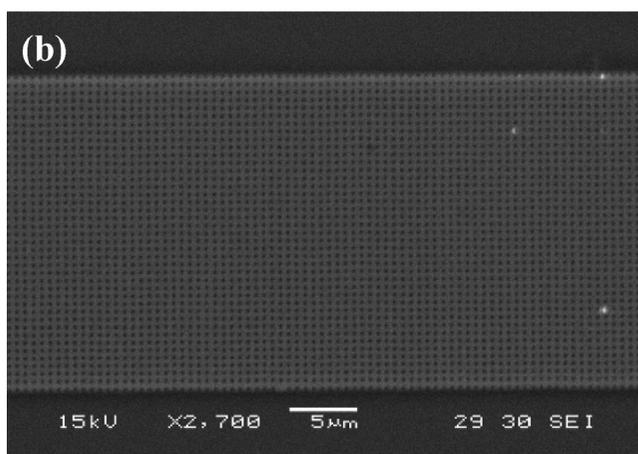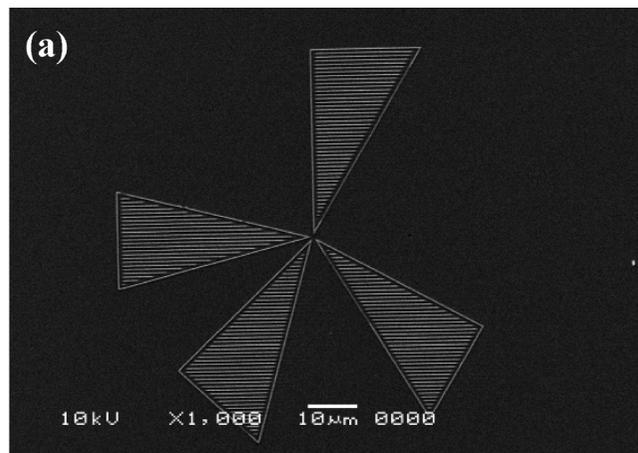
FIGURE 4. SEM images of PZT patterns by SCIL on Si(100) substrates after annealing at 650 °C in air: (a) pattern with a line width of 380 nm; (b and c) pit-patterned films, with pit diameters of 150 and 200 nm, respectively.
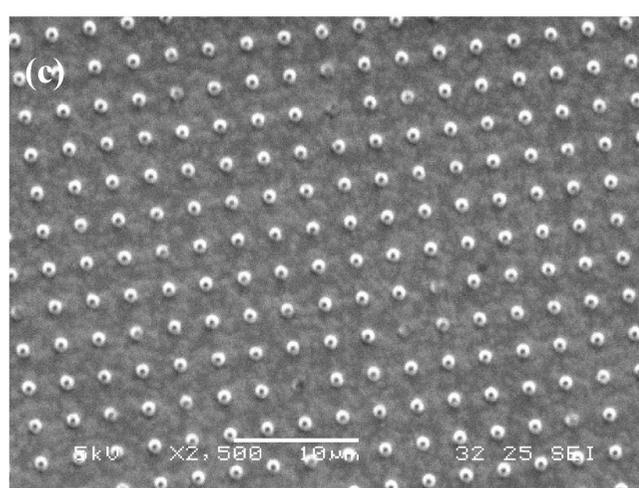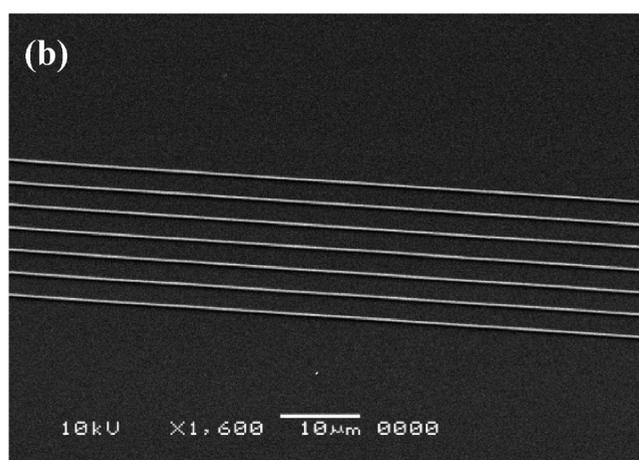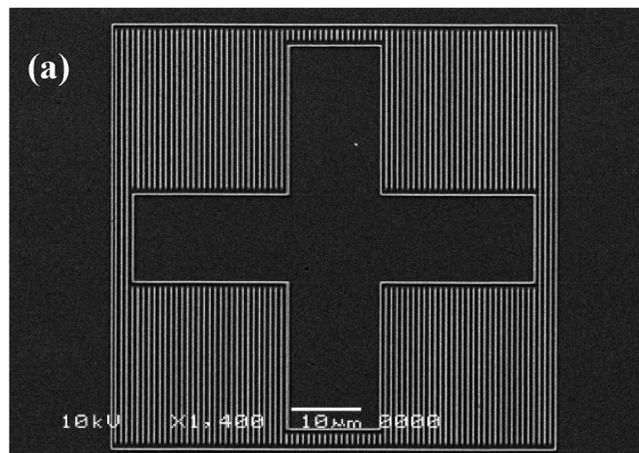

FIGURE 5. SEM images of PZT patterns by NTM on Si(100) substrates after annealing at 650 °C in air: (a) pattern with a line width of 380 nm; (b) line pattern with a line width of 100 nm; (c) array of nanodots with a feature size of 800 nm.

fied, the surface energy of the PDMS mold after plasma treatment should be higher than approximately 30 mJ/m^2 (γ_{sol}) and smaller than approximately 45−70 mJ/m^2 [$\sim 1/(2b + 1)\gamma_{SiO_x}$]. It is well-known that the surface properties of PDMS after oxygen plasma treatment are not stable. PDMS slowly regains its hydrophobic nature over time. This is due to diffusion of small oligomeric PDMS chains to the surface and/or adsorption of organic components from the gas phase. Both phenomena lead to an effective lowering of the

surface energy (32). We studied the changes in the contact angle of water on PDMS in air over time after 2 min of treatment in oxygen plasma. The contact angle changed considerably, from very hydrophilic just after the treatment to hydrophobic after ~24 h, as shown in Figure 3. The contact angle of untreated PDMS is shown for the sake of comparison. Indeed, the NTM experiments demonstrated that PDMS molds with very small contact angles for water (<10°) transferred much less of the patterning solution to
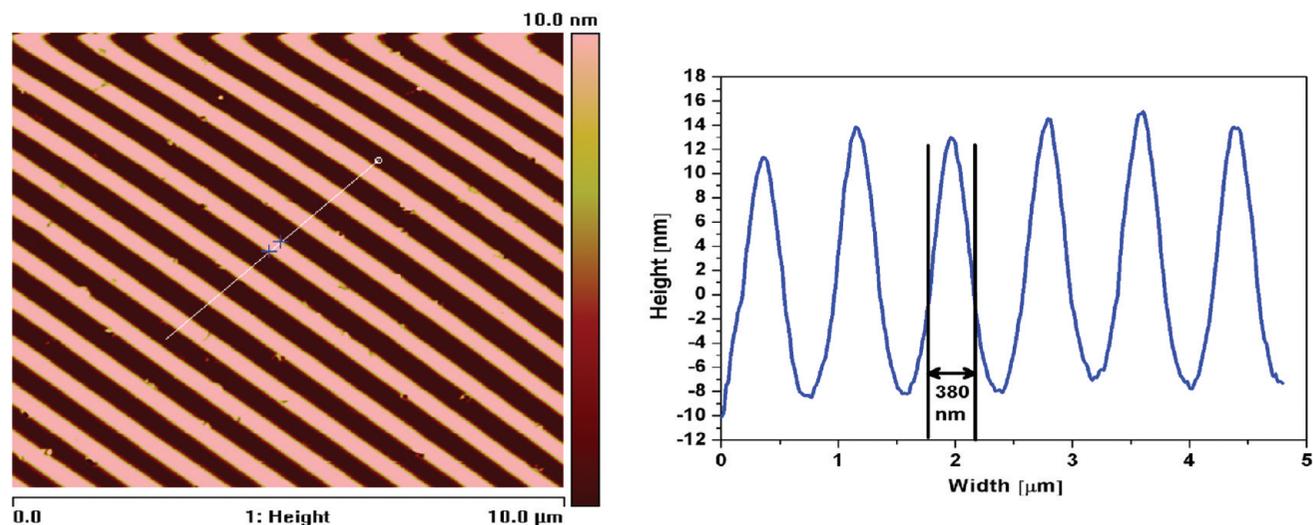
FIGURE 6. AFM height and section analysis of the PZT pattern obtained with the SCIL technique. The width is 380 nm; the height is approximately 25 nm.

the substrate than PDMS that had been plasma-treated for shorter periods of time. Under these conditions, the precursor adhered to the mold rather than to the substrate. We observed that plasma-treated PDMS with a water contact angle of ca. 30–40° gave good transfer of the PZT precursor sol to the substrate. Such a contact angle was accomplished by treatment of the PDMS mold in oxygen plasma for 10–20 s prior to use.

PZT Nanopatterns. Figures 4 and 5 show scanning electron microscopy (SEM) images of ceramic PZT patterns on silicon substrates fabricated by SCIL and NTM, respectively. All patterns were annealed for 10 min at 650 °C after an initial drying at 80 °C. It was observed that application of a pressure of ∼0.6 bar to the mold led to a significant improvement of the quality of the patterns and reduced the residual layer thickness. Although the flexibility of PDMS complicates the replication of features <200 nm (33), the low aspect ratios in this work and the low density of recessed features probably prevented stamp deformation from happening.

The elevated light-gray features in Figure 4a are a SCIL pattern with a line width of ca. 380 nm. Replication of the lateral shape of the features of the mold was very good. Various pit patterns with pit diameters in the range of 65–300 nm were also fabricated with SCIL. Figure 4b shows an overview of a pattern with a pit diameter of ca. 150 nm. Figure 4c shows a high-resolution SEM image of a pit pattern with a hole diameter of ca. 200 nm. The average PZT grain size was estimated from Figure 4c and appears to be in the range between 6 and 15 nm. As will be shown below, this corresponds well with estimates from XRD analysis. Figure 5 shows several PZT patterns obtained with NTM. The line width in Figure 5b is ca. 100 nm, and the length of the lines is 1 mm. In a few cases, the transfer process was not optimal, and adhesion of PZT features to the substrate was problematic, especially when nanodots were made. This is evident from a few missing dots in the array shown in Figure 5c. However, the adherence of line structures was good. It was also found that the residual layer between the patterned

lines is much thicker in SCIL than in NTM. This is due to the fact that the mold is directly imprinted into a continuous wet film in SCIL, while in NTM the sol is first transferred to the mold, after which all excess sol is removed from the protruding features. Obviously, less material will be present under the protruding features of the mold in NTM.

AFM was used to determine the height of the patterned features shown in Figures 4 and 5. Figure 6 shows AFM height images of the line patterns shown in Figure 4a. The results indicate that the maximum height is 25 nm. Interestingly, the line patterns do not have the double-peak profile observed in micrometer-scale MIMIC patterns (11). The difference is most likely related to the differences in the lateral dimensions of the patterns. In MIMIC, channel filling and sol drying occur simultaneously, and in micrometer-sized channels, the evaporation of solvent is considerably faster at the edges and in the corners of the channel. On the other hand, in imprinting and transfer-lithography techniques, the filling and drying are separated in time, while the effect of the much smaller feature size is that the drying process is much faster and occurs more homogenously throughout the sample.

It can be inferred from AFM analysis that the shrinkage of features in the vertical direction is comparatively larger than that in the horizontal direction. The height and width of the lines were reduced from 100 nm × 400 nm before drying to 25 nm × 380 nm after drying and heat treatment. This corresponds to a volumetric shrinkage of ∼24%. This value is close to the values reported by Vartuli et al. (10) for micrometer-sized PZT and by Beh et al. (34) for micrometer-sized ZrO_2 and SnO_2 line patterns. It was observed that two-thirds of the total volumetric shrinkage occurred in the primary stage of drying at 80 °C; the other one-third occurs at the thermal annealing stage.

Phase Analysis and Microstructure. Figure 7 shows θ–2θ spectra of a patterned PZT film after thermal annealing at 650 °C. All peaks correspond to the perovskite PZT phase and Si(100) substrate. The width of the XRD peaks was used to estimate the grain size d of a given
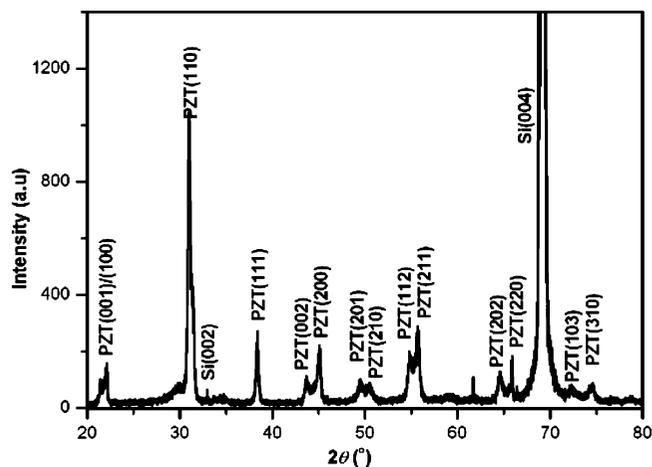
FIGURE 7. XRD pattern of the patterned PZT film on a Si(100) substrate.

powder, pattern, or film, by employing the Scherrer equation $d = 0.9\lambda/(W\cos\theta)$, where λ is the wavelength, W is the full width at half-maximum of the peak, and θ is the position of the respective XRD peak. The average grain size in the patterns was estimated from the PZT (111) peak and was found to be 8−10 nm. This is in good quantitative agreement with the grain size observed by high-resolution SEM, where a primary grain size of 6−15 nm was determined. Hence, the average PZT grain sizes are at least 1 order of magnitude smaller than the lateral dimensions of the pattern.

CONCLUSIONS

We demonstrated two soft-lithographic techniques with which PZT nanopatterns with a resolution down to 100 nm were made using flexible PDMS stamps. Both SCIL and NTM are promising for future nanofabrication of advanced functional oxides and composite materials, and the quality of the formed patterns was similar. The sol−gel precursor solution consisted of entities of ~2 nm or less, which is sufficiently small to be suitable for pattern replication of features of ~25 nm or more. The advantage of SCIL is that the requirements regarding the surface energies of the mold, substrate, and precursor solution are less strict than those with NTM and that adhesion between the substrate and PZT was good. The advantage of NTM is that much less residue stays behind between patterned features. The severe shrinkage of sol−gel-derived materials still remains a challenge. These patterns could be interesting for many applications, e.g., in nonvolatile memory devices, sensors, piezoelectrical materials, and nanoelectromechanical systems.

REFERENCES AND NOTES

(1) Scott, J. F. *Science* **2007**, *315*, 954−959.
(2) Scott, J. F.; Dearaujo, C. A. P. *Science* **1989**, *246*, 1400−1405.
(3) Moulson, A. J.; Herbert, J. M. *Electroceramics: Materials, Properties, and Applications*, 2nd revised ed.; Wiley: Chichester, U.K., 2003.
(4) Xia, Y. N.; Whitesides, G. M. *Annu. Rev. Mater. Sci.* **1998**, *28*, 153−184.
(5) Seraji, S.; Wu, Y.; Jewell-Larson, N. E.; Forbess, M. J.; Limmer, S. J.; Chou, T. P.; Cao, G. Z. *Adv. Mater.* **2000**, *12*, 1421−1424.
(6) Gobel, O. F.; Nedelcu, M.; Steiner, U. *Adv. Funct. Mater.* **2007**, *17*, 1131−1136.
(7) Yang, P. D.; Rizvi, A. H.; Messer, B.; Chmelka, B. F.; Whitesides, G. M.; Stucky, G. D. *Adv. Mater.* **2001**, *13*, 427−431.
(8) Heule, M.; Gauckler, L. J. *Adv. Mater.* **2001**, *13*, 1790−1793.
(9) Martin, C. R.; Aksay, I. A. *J. Electroceram.* **2004**, *12*, 53−68.
(10) Vartuli, J. S.; Ozenbas, M.; Chun, C. M.; Trau, M.; Aksay, I. A. *J. Mater. Res.* **2003**, *18*, 1259−1265.
(11) Martin, C. R.; Aksay, I. A. *J. Phys. Chem. B* **2003**, *107*, 4261−4268.
(12) Harnagea, C.; Alexe, M.; Schilling, J.; Choi, J.; Wehrspohn, R. B.; Hesse, D.; Gosele, U. *Appl. Phys. Lett.* **2003**, *83*, 1827−1829.
(13) Hampton, M. J.; Williams, S. S.; Zhou, Z.; Nunes, J.; Ko, D. H.; Templeton, J. L.; Samulski, E. T.; DeSimone, J. M. *Adv. Mater.* **2008**, *20*, 2667−2673.
(14) Verschuuren, M.; Van Sprang, H. In *Materials Research Society Symposium Proceedings*; Gigli, G., Ed.; Materials Research Society: Warrendale, PA, 2007; Vol. 1002, pp N03−05.
(15) Kim, J. H.; Lange, F. F.; Cheon, C. I. *J. Mater. Res.* **1999**, *14*, 1194−1196.
(16) Moran, P. M.; Lange, F. F. *Appl. Phys. Lett.* **1999**, *74*, 1332−1334.
(17) Yang, P. D.; Wirnsberger, G.; Huang, H. C.; Cordero, S. R.; McGehee, M. D.; Scott, B.; Deng, T.; Whitesides, G. M.; Chmelka, B. F.; Buratto, S. K.; Stucky, G. D. *Science* **2000**, *287*, 465−467.
(18) Schwartz, R. W.; Boyle, T. J.; Lockwood, S. J.; Sinclair, M. B.; Dimos, D.; Buchheit, C. D. *Integr. Ferroelectr.* **1995**, *7*, 259−277.
(19) Zhang, Q.; Huang, Z.; Whatmore, R. W. *J. Sol−Gel Sci. Technol.* **2002**, *23*, 135−144.
(20) Kim, W. S.; Kim, K. S.; Kim, Y. C.; Bae, B. S. *Thin Solid Films* **2005**, *476*, 181−184.
(21) Bras, W.; Dolbnya, I. P.; Detollenaere, D.; van Tol, R.; Malfois, M.; Greaves, G. N.; Ryan, A. J.; Heeley, E. *J. Appl. Crystallogr.* **2003**, *36*, 791−794.
(22) Zhang, Q.; Whatmore, R.; Vickers, M. E. *J. Sol−Gel Sci. Technol.* **1999**, *15*, 13−22.
(23) Boffa, V.; Castricum, H. L.; Garcia, R.; Schmuhl, R.; Petukhov, A. V.; Blank, D. H. A.; ten Elshof, J. E. *Chem. Mater.* **2009**, *21*, 1822−1828.
(24) Sekulic, J.; ten Elshof, J. E.; Blank, D. H. A. *Adv. Mater.* **2004**, *16*, 1546−1550.
(25) Mandelbrot, M. M. *The Fractal Geometry of Nature*; W. H. Freeman and Co.: New York, 1982.
(26) Teixeira, J. In *On Growth and Form*; Stanley, H. E., Ostrowsky, N., Eds.; Martinus Nijhof: Dordrecht, The Netherlands, 1986; pp 145−162.
(27) Teixeira, J. *J. Appl. Crystallogr.* **1988**, *21*, 781−785.
(28) Marzolin, C.; Smith, S. P.; Prentiss, M.; Whitesides, G. M. *Adv. Mater.* **1998**, *10*, 571−574.
(29) Hillborg, H.; Ankner, J. F.; Gedde, U. W.; Smith, G. D.; Yasuda, H. K.; Wikstrom, K. *Polymer* **2000**, *41*, 6851−6863.
(30) Ginn, B. T.; Steinbock, O. *Langmuir* **2003**, *19*, 8117−8118.
(31) David, B. A.; Seong, H. K. *J. Chem. Phys.* **2006**, *124*, 174712.
(32) Barbier, V.; Tatoulian, M.; Li, H.; Arefi-Khonsari, F.; Ajdari, A.; Tabeling, P. *Langmuir* **2006**, *22*, 5230−5232.
(33) Huang, Y. G. Y.; Zhou, W. X.; Hsia, K. J.; Menard, E.; Park, J. U.; Rogers, J. A.; Alleyne, A. G. *Langmuir* **2005**, *21*, 8058−8068.
(34) Beh, W. S.; Xia, Y. N.; Qin, D. *J. Mater. Res.* **1999**, *14*, 3995−4003.

AM900417Y